This is the peer-reviewed version of the following article:

Bajić, Z. J.; Veličković, Z.; Đokić, V.; Perić-Grujić, A.; Ersen, O.; Uskoković, P.; Marinković, A. Adsorption Study of Arsenic Removal by Novel Hybrid Copper Impregnated Tufa Adsorbents in a Batch System. *Clean-Soil Air Water* **2016**, *44* (11), 1477–1488. https://doi.org/10.1002/clen.201500765.

This work is licensed under a Creative Commons - Attribution-NonCommercial 2.0 Generic (CC BY-NC 2.0)

Accepted Article

Research Article

Adsorption study of arsenic removal by novel hybrid copper impregnated tufa adsorbents in a batch system†

Zoran J. Bajić[1], Zlate S. Veličković[1], Veljko R. Djokić[2], Aleksandra A. Perić-Grujić[2], Ovidiu Ersen[3], Petar S. Uskoković[2], and Aleksandar D. Marinković[2,*]

[1] Military Academy, University of Defense of Belgrade, Belgrade, Serbia

[2] Faculty of Technology and Metallurgy, University of Belgrade, Belgrade, Serbia

[3] Institut de Physique et Chimie des Matériaux de Strasbourg (IPCMS), UMR CNRS – Université de Strasbourg, Strasbourg, France

Correspondence: Professor A. D. Marinković, Faculty of Technology and Metallurgy, University of Belgrade, 4 Karnegijeva Street, 11120 Belgrade, Serbia

E-mail: marinko@tmf.bg.ac.rs

†This article has been accepted for publication and undergone full peer review but has not been through the copyediting, typesetting, pagination and proofreading process, which may lead to differences between this version and the Version of Record. Please cite this article as an 'Accepted Article', doi: [**10.1002/clen.201500765**].

© 2016 WILEY-VCH Verlag GmbH & Co. KGaA, Weinheim

Received: November 4, 2015 / Revised: April 6, 2016 / Accepted: July 18, 2016

Accepted Article

Abstract

Performance of a novel adsorbent, copper impregnated natural mineral tufa (T–Cu), applicable for efficient arsenic removal is presented in this study. Testing of adsorbent properties encompassed material characterization and equilibrium study in a batch system. Copper modification contributed to increased adsorption capacities, i.e., from 4.65 to 67.83 mg g^{-1} for As(III), and from 6.84 to 104.62 mg g^{-1} for As(V), comparing to unmodified tufa. The obtained thermodynamic data indicated higher feasibility and spontaneity of the adsorption process at higher temperature. A competitive study in a multi-component system showed that T–Cu adsorbents effectively removed arsenic species at high concentrations of interfering ions. The high adsorption capacity and multi-cycle reusability gave positive techno-economic indicators in comparison to commercial adsorbents.

Abbreviations: BET, Brunauer, Emmett and Teller; **BJH**, Barrett, Joyner and Halenda; **DW**, deionized water; **EDX**, energy dispersive X-ray; **EPA**, Environmental Protection Agency; **FEG-SEM**, field emission gun scanning electron microscopy; **FTIR**, Fourier-transform infrared; **HRTEM**, high resolution transmission electron microscopy; **iAs**, inorganic arsenic species; **ICP-MS**, inductively coupled plasma mass spectrometry; **MPC**, maximum permissible concentration; **PTFE**, poly(tetrafluoroethylene); **PZC**, point of zero charge; **RSM**, response surface methodology; **SAED**, selected area electron diffraction; **SEM**, scanning electron microscopy; **T–Cu**, copper impregnated tufa; **TEM**, transmission electron microscopy; **XRD**, X-ray diffraction

Keywords: Arsenite, Arsenate, Carbonate materials, Copper oxide, Water quality

1 Introduction

The presence of highly toxic arsenic compounds in the environment inevitably causes negative effect to human health. Exposure of human being to arsenic mostly occurs via use of contaminated water, although the other ingestion routes: inhalation, ingestion of food water, and dermal adsorption could not be neglected. Analysis of arsenic toxicology profiles, health effects and prevention of the exposure of human being to arsenic compounds are constantly growing tasks. Due to this, new criteria in assessing the quality of drinking water were issued reducing the maximum permissible concentration (MPC) from 50 to 10 μg L^{-1} [1]. The most abundant arsenic compound, found under oxic condition in nature is arsenate, As(V), while arsenite, As(III), mainly exists under anoxic condition. The highest toxicity of the As(III) species, comparing to arsenate, and several hundred times more toxicity than methylated arsenic compounds [2], indicate significance of the study related to inorganic arsenic species determination and removal from natural water.

The presence of arsenic in natural water comes from dissolution/transformation of minerals in the earth's crust or

Accepted Article

it could be the result of the leaching of arsenic compounds during mining/processing of metal ores from industrial/metallurgical complexes. In addition, application of agricultural pesticides or wood preservatives contributes to environmental pollution with arsenic. Due to this, throughout the world arsenic content temporarily/permanently exceed MPC in water, with the most serious problem recorded in south-eastern Asia, North and South America, and some regions in Europe [3--5]. Generally accepted and frequently used techniques for arsenic removal are coagulation and precipitation [6--9], nanofiltration and reverse osmosis [10-13], and ion-exchange and adsorption [14--28]. Simplicity of technological operation/manipulation and good/high efficiency of pollutant removal point to a selection of adsorption as one of the most appropriate methods applicable for arsenic removal [15, 21--28]. Extensive research, focused on the development of selective adsorbents for arsenic removal, was generally based on the use/modification of biological materials, mineral oxides, activated carbons, polymer resins, industrial by-products/wastes, soils, clays and sands [15, 29--30]. Regardless of the results achieved, there are still many disadvantages of the synthesized/designed adsorbents, and special care must be devoted to solving questions of safe disposal/processing of spent/exhausted adsorbent and generated sludge.

High affinity of copper oxide nanoparticles to both As(III) and As(V) (inorganic arsenic species, named iAs) was reported [31]. Effective arsenic removal was achieved over a wide pH range by using CuO nanoparticles. The interference of commonly present ions in natural water, namely silicate and phosphate, did not show significant detrimental effect on the effectiveness of arsenic removal. Moreover, uses of CuO do not require pH adjustments of inlet water and/or oxidation of As(III) to As(V) prior to adsorption step. High value of the point of zero charge of CuO nanoparticles, estimated at 9.4 ± 0.4 [31], significantly contributes to effective arsenic removal in a wide pH range. High adsorption capacity of copper nanoparticles in a batch system could not fulfill the performances required for practical application. Deposition of CuO on natural/synthetic supports could improve adsorbent performance [32]: textural properties, adsorption/kinetic performances, chemical stability, high affinity and selectivity with respect to arsenic.

Following such requirements, an optimal method was defined for the simultaneous reduction/precipitation of copper species on the natural material tufa in order to study adsorption performances of the novel hybrid material. The use of natural tufa was stimulated by its availability and low cost [29--31]. Main objectives of this paper were directed towards the production of a high performance adsorbent by studying: (1) morphological and textural properties, (2) sorption capacity, (3) equilibrium and thermodynamic aspects of the adsorption process, (4) effect of interfering ions, (5) long-term usability, and (6) certain aspects of the cost of the adsorption process.

2 Materials and Methods

2.1 Chemicals and standard solutions of arsenic and interfering ions

As(V) and As(III) stock solutions were prepared with deionized water (18 MΩ cm^{-1} resistivity) using $Na_2HAsO_4 \cdot 7\ H_2O$ (Sigma-Aldrich) and $NaAsO_2$ p.a. (J. T. Baker), respectively. Arsenic working solutions were freshly prepared by diluting the arsenic stock solutions with deionized (DW) water. The concentrations of arsenic species are always given as elemental arsenic concentrations in this study. Sodium silicate solution reagent grade (1.39 g mL^{-1}), sodium dihydrogen phosphate, NaH_2PO_4 (p.a.), sodium sulfate, Na_2SO_4, calcium nitrate, $Ca(NO_3)_2 \cdot 4\ H_2O$, magnesium nitrate, $MgNO_3 \cdot 6\ H_2O$, and potassium nitrate, KNO_3, trace metal basis chemicals were used (Sigma). $CuCl_2$, $NaBH_4$, NaOH (Sigma), HNO_3 (ultra-pure Fluka), and acetone for UV-spectroscopy (Fluka) were used as received. The initial standard As(III) and As(V) solutions, 1000 mg L^{-1}, were prepared by dissolution of the appropriate amount of sodium arsenite, $NaAsO_2$, and sodium arsenate, Na_2HAsO_4

Accepted Article

· 7 H_2O, in deionized water. The stock solutions preserved with 0.5 % trace of ultra-pure nitric acid could be stable for one year under an inert atmosphere and refrigerated. Solutions with concentrations of 0.1, 0.2, 0.3, 0.5, 1.0, 2.0, 3.0, 5.0 and 10.0 mg L^{-1} were prepared from the stock solution. In order to examine the influence of the ions usually present in water, a series of stock solutions containing appropriate concentrations of the anions sulfate, fluoride, nitrate, chromate and phosphate, and the cations nickel, zinc, cadmium and lead were prepared. These solutions were further diluted to suitable concentrations on the day of use.

2.2 T–Cu adsorbent preparation

Natural Tufa was collected in the area of Temska region, Pirot, Serbia. Tufa material, after milling and crushing in an agate mortar, was washed with deionized water (DW) in order to remove dusty materials, dried to constant weight and subsequently screened through a set of standard sieves. In this manner, three tufa fractions, A, B and C, were obtained. The obtained tufa fractions were washed three times with 200 mL DW, and dried in a vacuum oven at 90 °C for 6 h. Tufa samples coated with copper species were prepared by the chemical reduction of different copper(II) salts, i.e., chloride, nitrate, carbonate and sulfate, with sodium borohydride/sodium hydroxide. As an example: Tufa (20 g) was ultrasonicated in 100 mL of acetone for 1 h, and then magnetically stirred for 24 h followed by the addition of 250 mL of different concentrations of $CuCl_2$ in the range 0.4–1.2 mol L^{-1}. Reduction was performed by the simultaneous addition of different concentrations of $NaBH_4$ (150 mL), in the range of 0.1–0.2 mol L^{-1}, and 1 mol L^{-1} NaOH (250 mL) for 60 min with gentle mixing for 24 h. The solution pH affects the morphology of precipitated copper based nanoparticles and its adherence/binding to the tufa substrate [32]. Experiments were performed at 25, 35 and 45 °C. Detail on experimental design, by using response surface methodology (RSM) is given in Supporting Information Table S1. Obtained adsorbents were filtrated under vacuum, by using 0.2 μm pore size poly(tetrafluoroethylene) (PTFE) filter membrane, washed three times with DW, and dried at 70 °C for 24 h. After drying, the crushed material was sieved and three fractions were obtained: 0–0.02, 0.02–0.25, and 0.25–1.50 mm, samples T–Cu(A), T–Cu(B) and T–Cu(C) (Supporting Information Fig. S1).

2.3 Adsorbent characterization

Specific surface area, pore volume, and pore size distribution were obtained from the nitrogen adsorption–desorption isotherm measured using a Micrometrics ASAP 2020 V1.05H surface area analyzer by the Brunauer, Emmett and Teller (BET), and Barrett, Joyner and Halenda (BJH) methods. X-Ray diffraction (XRD) data were obtained by using a BRUKER D8 ADVANCE with Vario 1 focusing primary monochromator ($Cu_{K\alpha 1}$ radiation, λ = 1.54059 Å).

Fourier transform infrared (FTIR) spectra were recorded before and after arsenate adsorption at different initial arsenate and arsenite concentrations. The FTIR measurements were performed at room temperature in the transmission mode using a BOMEM (Hartmann & Braun) spectrometer. Determination of the zeta potential of the adsorbents was realized using a zeta potential analyzer (Zetasizer 2000, Malvern, UK). The pH values at the point of zero charge (pH_{PZC}) of the samples, i.e. the pH above which the total surface of the samples is negatively charged, were measured using the pH drift method.

Scanning electron microscopy with a field emission gun (FEG–SEM) was performed using a TESCAN MIRA3 electron microscope. The diameters of the nanocomposites were determined using MIRA TESCAN *in-situ* measurement software. Transmission electron microscopy (TEM) and high resolution TEM (HRTEM) analyses were performed on a Jeol 2100F (200 kV, Cs-corrected condenser, GIF Tridiem imaging filter) electron

Accepted Article

microscope.

The arsenic concentrations in the solutions after the adsorption and kinetic experiments were analyzed by inductively coupled plasma mass spectrometry (ICP-MS), using an Agilent 7500ce ICP-MS system (Waldbronn, Germany) equipped with an octopole collision/reaction cell, Agilent 7500 ICP-MS ChemStation software, a MicroMist nebulizer and a Peltier cooled (2 °C) quartz Scott-type double pass spray chamber. Standard optimization procedures and criteria specified in the manufacturer's manual were followed. ICP-MS detection limit was 0.030 μg L^{-1} and the relative standard deviation (RSD) of all arsenic species investigated was between 1.3–5.1 %.

2.4 Adsorption studies

Adsorption experiments were conducted in a batch system under ultrasonic and conventional stirring. The ultrasonic bath (Bandelin Electronic, Berlin, Germany, power 80 and 120 W, frequency 35 kHz) was thermostated by circulating water through the jacket. The batch adsorption experiments were conducted to study the optimum quantity, equilibrium time, effective pH range and the investigation of adsorption isotherms.

The effect of pH on arsenate and arsenite removal was determined by the addition of the adsorbent (100 mg L^{-1}) into the bottles containing 10 mL of 0.1 mg L^{-1} of arsenic solution. In order to evaluate the effect of pH on As(V) and As(III) adsorption, the initial pH values of solutions were varied from 3 to 10, adjusted with 0.1 mol L^{-1} NaOH and 0.1 mol L^{-1} HNO_3 at 20 °C. Adsorption isotherms of all adsorbents were obtained at pH 6.0 ± 0.1 for both As(V) and As(III) by varying the initial arsenic concentrations from 0.1 to 10 mg L^{-1}. All batch experiments, except when testing of the effect of temperature on arsenate adsorption, were performed at 20 ± 1 °C, adsorbent content of m/V = 100 mg L^{-1}, and ultrasonically-assisted treatment for 45 min. The influence of temperature on arsenate adsorption (20, 30 and 40 °C) was realized at pH 6.0±0.1. The adsorbent capacity was calculated according to Eq. (1):

$$q = \frac{C_i - C_f}{m} V \quad (1)$$

where q is adsorption capacity in mg g^{-1}, C_i and C_f are the initial and final arsenic concentrations in mg L^{-1} (μg L^{-1}), respectively, V is the volume of the solution in L, and m is the mass of the adsorbent (g). The desorption study was performed in the batch mode with various desorption agents: sodium hydroxide, sodium chloride, organic acid salt (formate, oxalate and citrate), at different concentrations: 0.1, 0.2, 0.5, 0.75 and 1 mol L^{-1} for 30, 60 and 90 min at 20 °C. The results showed that the adsorption of arsenate and arsenite on the glass tube wall and filters was negligible.

2.5 Experimental design of T–Cu preparation by using RSM

RSM optimization of Tufa fabrication was based on five-level-three-factor central rotatable composite design. The concentrations of $CuCl_2$ and $NaBH_4$, and the temperature were the three independent variables. The coded and operational values of the selected variables are shown in Supporting Information Table S1, together with the experimental plan, which comprised 16 experimental runs plus six replicates on the central point [33]. Each experiment (except the central point) was performed in duplicate. The output variable was the adsorption capacity of the obtained adsorbent. Data obtained in these experiments were fitted with a second-order polynomial equation and the coefficients of the response function and their statistical significance were evaluated by the least squares method using MATLAB software R2012B, (The MathWorks, Juc, Matick, MA, USA). The Fisher test was used to determine the adequacy of the model and the Student distribution to evaluate

the significance of the coefficients.

2.6 Statistical analysis of the experimental data (error analysis)

In order to select the most appropriate isotherm and kinetic models, i.e. to confirm the successfulness of the fitting of the experimental data, it was necessary to perform error analysis together with the determination of the values of the correlation coefficient (r), obtained from the regression analysis. The adsorption experiments were performed in triplicate, and only mean values are reported. The kinetic, isotherm and thermodynamic parameters and their standard errors were calculated, applying linear and/or non-linear least-squares methods, using commercial software (Microcal Origin 8.0). The non-linear isotherm modeling has numerous benefits over linearization models: the involvement of the minimization or maximization of error distribution between the experimental data and the modeled isotherm based on its convergence criteria.

The error data analysis was realized according to the average relative standard error (ARS), the sum squares error (ERRSQ/SSE), the Marquardt percent standard deviation (MPSD), hybrid fractional error function (HYBRID), average relative error (ARE); normalized standard deviation (NSD), standard deviation of the relative errors (S_{RE}), the Spearman correlation coefficient (r_s), and the non-linear chi-square test (χ^2). HYBRID was developed to improve the fit of the square of the errors function at low concentration values. The *MPSD* is similar in some respects to a geometric mean error distribution modified according to the number of degrees of freedom of the system. The root mean squared error test and the non-linear χ^2 test are two mathematical error functions used in this study to determine the best fitting of the adsorption model.

3 Results and Discussion

3.1 Optimization procedure for adsorbent preparation

An optimization procedure was conducted in order to obtain an adsorbent of high adsorption efficiency, and improved chemical and mechanical stability of the copper tufa coverage. Comparison of the adsorbents performances, prepared with different copper salts, showed that the best characteristics were obtained using copper(II) chloride. The obtained results revealed that the optimal adsorbent performance was obtained with 1.0 mol L^{-1} $CuCl_2$ and 0.16 mol L^{-1} of $NaBH_4$ at 25 °C (Fig. 1). The optimization goal, i.e., the maxima adsorption capacities with respect to As(V), was obtained at 4 % loaded copper (≈5 % calculated as CuO) (Fig. 1b). The small maximum adsorption capacity (q_{max}), given in Fig. 1b, is due to low initial adsorbate concentration (C_i = 0.1 mg L^{-1} As(V)). T–Cu(B and C) were prepared in an analogous way as T–Cu(A).

3.2 Tufa and T–Cu(A) characterization

The elemental composition of unmodified tufa and T–Cu(A) are given in Supporting Information Table S2. The textural properties, pH_{PZC} and zeta potential values of tufa and T–Cu(A-C) were determined using ICP, BET/BJH, the drift method and zeta potential analyzer, respectively, and the results are presented in Table 1.

It is noticeable from the elemental composition (Supporting Information Table S2) that tufa basic material contains an appropriate amount of iron oxide. It was expected that tufa, according to evidenced good affinity of iron oxide to arsenic species [30], could be good supporting material for further modification with reduced/precipitated copper species. Improvement of textural properties of T–Cu adsorbents was also noticed after modification. Improvement of textural properties of T–Cu adsorbents was also noticed after modification. The textural parameters of tufa and T–Cu adsorbents, i.e., the specific surface area (S_p), pore volume (V_p), average pore diameter, and the pH_{PZC} and zeta potential are given in Table 1.

Accepted Article

Accepted Article

Precipitation of reduced copper species created a nano-scaled deposit with improved textural parameters of T–Cu adsorbents (Table 1). Significant increase in the surface area and porosity of T–Cu adsorbents is due to the beneficial ratio of surface area/pore diameter to the nanoparticles volume of precipitated copper based precipitate [34]. Modification of the three tufa fractions showed that the surface area moderately decreased from 65.47 for T–Cu(A) to 46.89 m^2 g^{-1} for T–Cu(C), and the mesopore volume decreased from 0.336 for T–Cu(A) to 0.285 mL g^{-1} for T–Cu(C). The modified tufa showed higher values of the mesopore diameter (almost 2.2 times greater), with a slight decreasing trend from T–Cu(A) to T–Cu(C) (Table 1). The higher values of the isoelectric point of the T–Cu adsorbents means that the positively charged surface is the driving force for arsenic adsorption over a wide pH range. Moreover, the moderate decrease in the pH_{PZC} value after adsorption, from 8.1 ± 0.3 to 7.2 ± 0.4, indicated that specific arsenate adsorption is of major contribution to the overall adsorption process [35], i.e. processes of surface complexation predominate over electrostatic interactions.

3.3 X-ray diffraction patterns (XRD) analysis

The XRD patterns of T–Cu(A) are given in Fig. 2.

X-Ray powder diffraction analysis was used for phase and structure determination. The strong $CaCO_3$ peak at 2θ = 29.5 (ICDD PDF2 No. 85-1108) was manifested in both tufa and T–Cu XRD patterns. Furthermore, $CaCO_3$ peaks were evident at the 2θ angles of 39.5, 47.6, 48.6, 57.5, 60.8 and 64.8. Monoclinic SiO_2 (ICDD PDF2 No. 89-1813) showed a notable peak at the 2θ angle of 23.8 only for tufa; the peaks for T–Cu were of considerably lower intensity. Hexagonal SiO_2 (α-SiO_2) (ICDD PDF2 No. 85-0865) showed four notable peaks for both tufa and T–Cu at 26.7, 36.7, 39.5 and 60.1. Copper(I) and (II) compounds used for T–Cu were CuCl (ICDD PDF2 No. 77-1996), $CuO{\cdot}3H_2O$ (ICDD PDF2 No. 36-0545) and Cu(OH)Cl (ICDD PDF2 No. 13-1063). CuCl showed peaks at the 2θ angles of 28.1 and 46.8, while $CuO \cdot 3 H_2O$ exhibited peaks at 24.3 and 34.1 and Cu(OH)Cl at 15.9 and 32.4. From the XRD pattern of T–Cu(A) the crystallite size of deposit materials on bigar surface was determined according to the Scherrer equation, Eq. (2) [36]:

$$D = K\,\lambda/(\beta\cos\theta) \quad (2)$$

where λ is the wavelength of the X-ray radiation (λ=1.54059 Å), K is the Scherrer constant (K = 0.9), θ is the angle of characteristic X-ray diffraction peak (θ = 12.65°) and β is the full-width-at-half-maximum of the most intense peak (in radians). The average size of the CuCl, $CuO{\cdot}3H_2O$ and Cu(OH)Cl particles were calculated to be 8.8, 11.5 and 11.4 nm, respectively.

3.4 Morphological characterization

The morphological characterization of nanostructural deposit of the T–Cu(A–C) samples were studied by using FEG–SEM (Fig. 3 a–c) and TEM/HRTEM techniques (Fig. 3d and Supporting Information Fig. S2). Selected area diffraction pattern (SAED) and dark field images of T-Cu(A) are given in Supporting Information Fig. S3.

The results of the SEM analysis (Fig. 3) showed that the particles were sphere-like with corrugated T–Cu grains and prominent non-uniformity on the surface. According to MIRA TESCAN in-situ measurement software, the mean diameter of adsorbent aggregates were evaluated to be 6.4 ± 2.2 μm for T–Cu(A), 64.6 ± 14.8 μm for T–Cu(B) and 780 ± 187.6 μm for T–Cu(C). The applied treatment under mild reducing conditions did not cause etching of the tufa surface, but instead led to slight increases in the grain diameters and higher porosities introduced by the formation of the deposit on the tufa surface.

Analysis of HRTEM images, taken on several representative aggregates of the T–Cu(A) specimen, showed the presence of crystallized nanometric grains located at the surface of the aggregate. Several inter-planar distances

Accepted Article

of the crystallographic grains, corresponding to the copper and copper oxide structures, were defined from HRTEM analysis. The example of SAED pattern, taken on one of the typical aggregates of T–Cu(A), is shown in Supporting Information Fig. S3. By indexing this pattern, one can observe that it corresponds to a superposition of two crystallographic structures, namely the metallic and copper oxide structure, confirming the results obtained from XRD analysis. In addition, to identify the geometrical characteristics of the crystalline parts of the aggregate, an intense area from the pattern which contains two diffraction spots was selected, and acquired dark field image is given in Supporting Information Fig. S3 c. This image allows to observe two types of crystallographic grains: first, large grains, with a mean size of about 10 nm, corresponding to the metallic copper, and the second, smaller grains, with nanometric size of 1--2 nm, which can be assigned rather to copper oxide. According to the analysis of the HRTEM images taken on few aggregates of the T–Cu(A)/As specimen (Supporting Information Fig. S2), some crystalline grains can be observed, similarly to the T–Cu(A) sample, but having slightly larger diameters, between 10 and 20 nm, instead of 10 nm observed for the T–Cu(A) sample. The analysis of the crystallographic distances allows once again to assign the crystallographic parts of the aggregate to the presence of both metallic and oxide copper structures.

3.5 FTIR analysis

Representative FTIR spectra of tufa, T–Cu(A), T–Cu(A)/As(V) and T–Cu(A)/As(III) are given in Fig 4. Three main peaks at 1429, 877 and 709 cm^{-1} were observed in the FTIR spectrum of the unmodified tufa (Fig. 4a). Among them, the very strong band at 1429 cm^{-1} was assigned to the C–O stretching mode of carbonate explained that the vibration modes of calcium carbonate showed three main IR bands, ≈714 cm^{-1} (ν_4, in-plane bend), ≈879 cm^{-1} (ν_2, out-of-plane band) and ≈1432 cm^{-1} (ν_3, asymmetric stretching), and one inactive band, ≈1097 cm^{-1} (ν_1, symmetric stretching) [37]. In the FTIR spectra of the tufa particles, due to the presence of the silica phase, the absorption bands at ≈1097 cm^{-1} is the result of overlapping bands from calcite and the asymmetric vibration of the Si–O group. Moreover, the asymmetric vibration of Si–OH appeared at 950 cm^{-1}, and symmetric vibration of Si–O at 795 cm^{-1}. Three peaks of low intensities, observed at 1090, 1043 and 950 cm^{-1}, were ascribed to the bending vibration of hydroxyl groups present at the surface of the iron oxide phase (Fe–OH). In addition, the appearance of a band at 636 cm^{-1} confirmed the presence of Fe–O bonds in iron oxide structure exposed at the tufa surface. The presence of surface hydroxyl groups was confirmed by an intense absorption band at 3433 cm^{-1}, assigned to the O–H stretching vibration, and by the band that appeared as a shoulder at 1633 cm^{-1}, which corresponds to the bending vibration of O–H groups.

The bands visible on the spectrum of tufa starting material (Fig. 4a) were shifted or found to be of lower intensity, while some had completely disappeared after modification (Fig. 4b). The concomitant appearance of new bands indicated changes the surface functionalities, i.e., indicates presence of new phases. The FTIR bands of the CuO deposit (Fig. 4b) showed three main vibrational modes observed at 472, 535 and 590 cm^{-1}, whereas the broad absorption band at around 618 cm^{-1} is attributed to the Cu–O vibration of copper oxide. For CuO nanoparticles, a high frequency mode at 590 cm^{-1} was reported due to Cu–O vibration stretching along the [–101] direction [32]. The FTIR results confirmed that a copper coating at the tufa surface provided bonding/complexing sites for the removal of arsenic species.

A comparison of the FTIR spectra of the unmodified and modified tufa with those obtained after As(V) (Fig. 4c) and As(III) (Fig. 4d) adsorption showed that the surface complexation of arsenic species changed the FTIR absorptions of the host lattice. A weakening of the band at 1115 cm^{-1} could be observed, which almost disappeared when the concentration of As(V) reached 5 mg L^{-1}. After As(V) adsorption, a new absorption band,

Accepted Article

corresponding to the As–O stretching vibration of coordinated arsenic species, appeared at 823 cm^{-1}. The shorter bond distance resulted in a stronger force constant and, consequently, a higher infrared frequency, and thus the stretching vibration of uncomplexed/unprotonated As–O–Fe is located at a higher position (860 cm^{-1}), while the frequency of the complexed As–O–Fe band is located at lower frequency (823 cm^{-1}) [37]. The lower intensities absorption bands changes could be noticed from the FTIR spectrum given in Fig. 4d.

3.6 pH sensitivity of arsenite and arsenate adsorption by T–Cu(A)

Due to the important role of the pH on the speciation of arsenic (Supporting Information Fig. S4) and the ionization of the adsorbent surface, it was necessary to determine the optimal operating pH for arsenic removal. The pH-dependent adsorption of As(III) and As(V) were found to follow a similar trend (Fig. 5). Evaluation of the successfulness of the most convenient techniques commonly applied for pollutant removal, classical stirring and ultrasound treatment (denoted as m and u, respectively, in Fig. 5), were performed. Intensification and effectiveness of the diffusional processes in an adsorption system, subjected to an ultrasound source, was influenced by improved material wetting and lower resistivity of mass transfer [37, 38]. Due to higher adsorption capacity, by 5–15 % in the case of magnetic stirring, it was appropriate to select this technique for the adsorption experiments.

Arsenic acid has pK_a values 2.3, 7.0 and 11.5 and it exist mainly as anionic species ($H_2AsO_4^-$ and $HAsO_4^{2-}$) at wide range of pH (Supporting Information Fig. S4). Arsenous acid, with dissociation constants pK_a of 9.2, 12.1 and 13.4, is present mainly as neutral species at pH < 9 (Supporting Information Fig. S4). A low dependence of the removal efficiency on pH was also found for arsenate and arsenite, and the percentage removal ranged between 98 and 96% for arsenate, while arsenite removal was in the range of 87 and 78 % in the pH region of 3–6. Accordingly, pH 6 was selected for both As(III) and As(V) as the optimal value and used in the following experiments.

At pH < pH_{PZC}, the protonation of surface functional groups takes place at significant extent and thus, the generated positive charge at the adsorbent surface contributes to favorable bonding of negatively charged arsenate ions. Enhancement of electrostatic attraction is thus highly feasible for As(V) species, while it is of minor importance for the neutral form of arsenous acid. The polarizable structure of arsenous acid could be susceptible to participation by lower intensity electrostatic interactions with functionalities at the adsorbent surface. According to the results of the pH-dependent adsorption study, when initial pH value (pH_i) was lower than pH_{PZC}, $pH_i < pH_{PZC}$, efficient arsenic removal is due to the contribution of complexation and electrostatic attraction, i.e., ionic, dipolar and hydrogen bonding interactions. At $pH_i > pH_{PZC}$, the contribution of both deprotonation of surface functional groups and the concentration of negatively charged arsenic species contributed to enhanced repulsion at the boundary layer of the adsorbent interface.

3.7 Adsorption study

Influence of pH on adsorption efficiency of T–Cu(A) for arsenic removal is presented in Fig. 5, according to which, the effective removal of As(V) could be accomplished at pH 4–7 [16, 38]. At the operating pH, favorable electrostatic interactions between the surface active sites and arsenic species contributed to the selective binding of arsenic species. Moreover, this pH value is usually found in natural water, which facilitates possible implementation of the technology in practice. From the techno-economic aspect, the possibility of using untreated natural water (without pH adjustment) would have a significant beneficial impact on the capital and operational costs of the implemented technology.

Accepted Article

Various isotherm models [39--41] were used to analyze adsorption processes and evaluate the adsorption capacity of T–Cu adsorbents. Additionally, in order to select the best adsorption isotherm model, a statistical validity of the modeling was estimated from the results of comprehensive error analysis. The results of the linear and non-linear fitting of experimental data are given in Table 2 for T–Cu(A) (Fig. 6), and in Supporting Information Tables S3 and S4 for T–Cu(B) and T–Cu(C) adsorbent, respectively. It was found that the Jovanovic–Freundlich and Sips models gave the best fitting for T–Cu(A) and T–Cu(B) for both As(III) and As(V), and Jovanovic and Sips for As(III) and As(V) regarding T–Cu(C) (Supporting Information Tables S5 and S6). The results of modeling of the experimental data using the Langmuir isotherm showed the high predicted maximum adsorption capacity on T–Cu(A): 67.83 mg g^{-1} for As(III) and 104.62 mg g^{-1} for As(V) (Table 2), and a decreasing trend with increasing average diameter of T–Cu(B) and T–Cu(C) could be noticed (Supporting Information Tables S3 and S4). The obtained results are in accordance with the positive zeta potential of CuO which contributes to higher affinity of the T–Cu to iAs: literature finding is 31 mV at neutral pH [30, 31] and 16.5 mV was found at pH 6 for T–Cu (Table 1).

Due to beneficial textural properties, i.e. ratio of surface area/pore volume/pore diameter of T–Cu(A–C) adsorbents, a large number of the adsorption sites are situated at external adsorbent surface and volume/pore diameter of interior pore network are favorable to provide lower resistivity to arsenate diffusion transport.

The evaluation of adsorption performances and possible application of T–Cu(A–C) adsorbents was deduced from a comparison with literature data collected and presented in Supporting Information Table S7. Special care was related to comparison with copper-based [42--45], and iron oxides based adsorbents [35, 37]. Comparison with iron oxides based adsorbent was performed due to well-known fact that modification of substrate with iron oxyhydroxides produce high affinity materials applicable for arsenic removal [30, 35, 37]. Differences in the experimental conditions allow only a general qualitative overview of the analyzed adsorption data. Nevertheless, a short comparative analysis of literature data (Supporting Information Table S7) with respect to q_{max} obtained for T–Cu(A–C) adsorbents (Tables 2 and Supporting InformationTables S3 and S4) is presented. Copper(II) oxide nanoparticles [42,43] and CuO incorporated on mesoporous alumina [45] are adsorbents with similar to larger surface areas (Supporting Information Table S7) than those found for T–Cu(A–C) adsorbents (Table 1). Regardless to beneficial textural properties of these adsorbents, a low adsorption capacities capacity of 1.086 mg g^{-1} [42] and moderate capacity of 26.9 and 22.6 mg g^{-1} [43], for differently synthetized CuO nanoparticles, were obtained. It is also noticeable that CuO incorporated on mesoporous alumina [45], an adsorbent with high surface area, 189.25 m^2 g^{-1}, showed a low capacity of ~2 mg g^{-1} (Supporting Information Table S7). Iron oxides based adsorbents shows lower adsorption capacities, e.g. highest value of 50 mg g^{-1} was found for maghemite nanoparticles (Supporting Information Table S7). Detail explanation on the origin of presented adsorbents, properties and obtained adsorption capacities is given in the Supporting Information. It was also recently shown that modification of egg-shell calcite and synthesized calcite with goethite gave moderate adsorption capacity for As(V) removal: 33.38 mg g^{-1} [35] and 21.00 mg g^{-1} [37] which are lower values than those obtained for the T–Cu(A–C) adsorbents (Table 2). Based on the presented results and previous findings [33], appropriate relationship between textural parameters and adsorption capacity could be postulated. Except of the preferable textural properties, which contributed to increased availability of surface active sites and increased intra-particular diffusional transport, also pronounced affinity of modifying deposit could be more influential factor. All of these factors contribute to better performance of T–Cu(A–C) adsorbents than copper based adsorbents and ones obtained from natural renewable materials (Supporting Information Table S7). The presented results indicated that the most significant feature of prepared T–Cu(A–C) adsorbents lies in beneficial textural

properties (Table 1) and high affinity of copper based nanodeposit obtained according to optimized method.

3.8 Thermodynamic study

The Gibbs energy (ΔG^0), enthalpy (ΔH^0), activation energy (E_a) and entropy (ΔS^0) of adsorption were calculated using the van't Hoff equations [35]:

$$\Delta G^0 = -RT \ln b \quad (3)$$

$$\ln b = \Delta S^0 / R - \Delta H^0 / (RT) \quad (4)$$

where T is the absolute temperature (K) and R is the universal gas constant (8.314 J mol^{-1} K^{-1}). The Langmuir sorption constant b was derived from the isotherm experiments. ΔH^0 and ΔS^0 can be obtained from the slope and intercept of the linear plots of ln$b$ versus T^{-1}, respectively, assuming the sorption kinetics to be under steady-state conditions. The calculation of thermodynamic data was based on the results obtained from adsorption isotherms data modeling (Table 3).

The negative standard free energy changes (ΔG^0) indicated greater feasibility for adsorption at higher temperatures, while positive standard entropy changes (ΔS^0) indicate a higher overall disorder of the system at equilibrium, i.e. adsorption is an entropy-driven process. Low dependences of all thermodynamic parameters on adsorbent size could be noticed. The high negative ΔG^0 values indicate that bidentate binuclear inner sphere complexes dominate as bonding arsenate species on adsorbent surfaces. At higher temperatures, disruption processes of the arsenic oxyanion hydration shell and transport of exchangeable arsenic oxyanions to the adsorption sites, on the one hand, and the number of water molecules released into the bulk solution, on the other hand, contribute to increases in the entropy change [46, 47]. The increased entropy of the system under steady-state conditions is presumably due to increased randomness at the adsorbent/solution interface. i.e., contribution of different intermolecular interactions between the molecule/groups present on the adsorbent surface [35]. All the elementary processes of mass transport that occur during equilibration of the system, from an energetic point of view, contribute to a positive enthalpy change.

3.9 Influence of competing anions on T–Cu(A) adsorption in a batch system

The important objective of the present study was devoted to evaluation of the usefulness of T–Cu(A–C) adsorbents in the presence of ions commonly present in natural water: anions as chloride, sulfate, fluoride, nitrate, chromate and phosphate, and cations as nickel, zinc, cadmium, lead and silica. Evaluation of the detrimental effect of interfering ions on the effectiveness of As(V) and As(III) removal using the T–Cu(A) adsorbent was realized. The model water spiked with 100 μg L^{-1} of As(V) and As(III) and competitive ions, concentrations similar to those found in natural water, was used in this study, and the results are presented in Table 4 and Supporting Information Table S8, respectively.

The presence of interfering ions even at high concentrations caused only a slight decrease in the effectiveness of As(V) and As(III) removal by the T–Cu(A) and T–Cu(B) adsorbents. Of all commonly present anions, sulfate and phosphate, divalent and trivalent anions, respectively, showed greatest detrimental effect on iAs adsorption at higher pH values.

The results of the competitive study of iAs removal in the presence of cations by T–Cu(A and B) are presented in Supporting Information Table S8. It should be emphasized that noticeable adsorption of silica, Zn and Pb occurred, while slight concentration decreases of Mn, Cd and Ni took place simultaneously with arsenic species removal. Arsenate, and to a lesser extent arsenite showed low sensitivity to ionic strength changes: increased

Accepted Article

Accepted Article

adsorption with increasing ionic strength of solution suggests that the primary adsorption mechanism was the formation of inner-sphere complexes within the coordination sphere of the adsorbent surface, and also electrostatic interactions play an appropriate role in the overall adsorption process. It is also important to assess the leaching properties of the used adsorbent into the effluent water during adsorption. The water quality parameters, including effluent copper concentration, showed low alternation with a slight pH change, with the exception of low increase of the total dissolved solids. Low value of leached copper determined after treatment with T–Cu(A), found at the level of <45 μg L^{-1}, confirmed that the amount of copper is below the United States Environmental Protection Agency (US EPA) limit of 1.3 mg L^{-1} [35].

3.10 Adsorption/desorption study *versus* safety

Due to the necessity to provide long-term adsorbent exploitation, a reusability study was performed with variable process parameters: concentration, time and regenerator type. In order to minimize the impact of material cost, development of high capacities, long-term adsorbent use, and successful regeneration technology provide a high performance adsorbent for practical applications. The regeneration efficiency, i.e., the number of the cycles of adsorbent reuse, largely contributes to cost effectiveness of an adsorption process. The development of efficient regeneration technology would help prevent the generation of spent contaminated adsorbent. This fact will be considered in a techno-economic analysis before possible practical applications, i.e., scale-up of adsorbent synthesis and development/-implementation of the technology in practice.

In order to design high-performance adsorbents, and to select effective desorption agents it was necessary to assume possible adsorption/desorption mechanism, which is given in Supporting Information Fig. S5. The consideration was based on literature results and those presented here. X-Ray photoelectron spectroscopy (XPS) analysis of the samples obtained by adsorption of As(III) and As(V) onto CuO nanoparticles indicated that As(III) adsorption takes place by a two-step mechanism: oxidation As(III) to As(V) and adsorption [45]. Also, it was found and confirmed in this work, that As(III) removal is affected at higher extent by the presence of interfering ions (Table 4 and Supporting Information Table S8). This is an additional evidence of a multi-step adsorption process. The decrease of pH_{PZC} for T–Cu(A-C), from 8.1 ± 0.3 to 7.2 ± 0.4, indicated that specific adsorption dominates over electrostatic interactions. The increases of adsorption capacities of T–Cu(A–C), in the temperature range of 20–40 °C (Table 3), indicate a complex adsorption mechanism and time-dependent changes in the contribution of physisorption and chemisorption: ion exchange/electrostatic attraction and surface complexation/precipitation processes, respectively, to the overall adsorption process. Based on such assumption appropriate selection of desorption agents were done, and their efficiency was studied in desorption experiments. Strong bases and acids are the most efficient regenerators of exhausted adsorbents. The selection of the regenerator is dictated primarily by the bonding type of arsenic species at the adsorbent surface; hence different desorption agents were used in a desorption study (Supporting Information). The desorption study showed that hydroxide ions, OH^-, strongly compete with bonded arsenic species to occupy adsorbent surface. The results of the desorption study, obtained by using different concentration/ratio of the sodium hydroxide/-sodium chloride system, are given in Table 5. Desorption efficiency represents percent of the amount of arsenic desorbed to the amount of arsenic adsorbed per mass unit of adsorbent.

Higher pH is favorable for efficient deprotonation of bonded arsenate which is in turn more susceptible to be exchanged with hydroxyl ions. Due to this, the NaOH/NaCl (0.5:0.5) system showed highest desorption efficiency (Table 5) with 89% desorbed arsenate in the first cycle of the regeneration process. According to the results of iAs desorption, it could be noticed that As(V) was tighter bonded to the surface of T–Cu(A). The

Accepted Article

collected spent alkaline solution from the regeneration process contained relatively high amounts of arsenic that necessitates the application of a short and simple technology developed for the transformation of the collected effluent into a safe material suitable for appropriate land filling. The most effective technology for safe disposal of desorption solution and washing medium could be treated by iron(III) chloride solution (5%) with pH adjustment at 7 using 15 % hydrochloric acid. After standing for 12 h, a heavy brown precipitate formed, which could be easily filtered of using a combination of coarse (top) and fine (down) sand filters mixed with some filtration aid - diatomaceous earth. The toxicity characteristic leaching procedure was applied to evaluate hazardous characteristic of the exhausted adsorbent and sludge which could be safely handled and disposed of in landfills. The iAs concentration was <5 mg L^{-1} established by the US EPA standard, which indicated possible safe disposal of the exhausted adsorbents.

3.11 Short techno-economic analysis

Techno-economic analysis of a newly synthesized adsorbent and the overall cost of the technology in use are important parameters that are key criteria which must be considered at a decisive point before commencing work on the study and design of arsenic removal at the pilot and full-scale level of application. Details on main categories and methodology used in techno-economic analysis are given in the Supporting Information.

The price of Lewatit FO36 is about 1.5 $/kg (1.32 €/kg), far higher than the production costs of T–Cu(A). Assuming similar operational and regeneration costs, this means that a comparative analysis could be based on simply the cost of adsorbent per gram of arsenic removed from water. By applying such a calculation, it was shown that these costs are 0.006 and 0.21 €/g As(V) for T–Cu(A) and Lewatit FO36, respectively. These simplified calculation indicates the favorable properties/cost relationship for T–Cu(A) and its outstanding opportunities for application in a real water purification system. Such an analysis requires confirmation in a future study including a fixed-bed column investigation and detailed techno-economic analysis. Therefore, in the present study, high capacity and good affinity adsorbents used for arsenate removal from natural water were synthesized. Efficient arsenic removal was achieved even at high concentrations of interfering ions. Positive economic indices regarding possible application in a real water purification system are justified. The obtained results indicate that T–Cu could be acceptable alternative to commercial expensive adsorbents currently in use.

4 Concluding Remarks

In summary, a highly efficient low-cost adsorbent for arsenic removal was obtained by precipitation of reduced copper species on the naturally widespread material tufa. The results of pH studies reveal that obtained T–Cu adsorbents showed high adsorption affinity with respect to arsenic species over a broad pH range. Modeling of the adsorption equilibrium data helped in understanding the relation between the adsorbent properties and adsorption parameters/processes. A comprehensive statistical analysis aided in the proper selection of the isotherm model. Thermodynamic parameters revealed that the adsorption processes were favorable and more spontaneous at higher temperatures.

The experimental results showed that the used adsorbent was efficient and reusable for arsenic removal from natural water in the presence of interfering ions commonly found in natural water. The experimental results showed that the used adsorbents were efficient and reusable for arsenic removal from natural water in batch operational mode. The possible use of natural material tufa is justified/stimulated by its natural origin, availability, and low cost.

Accepted Article

Acknowledgment

The authors acknowledge the financial support from the Ministry of Education, Science and Technological Developments of the Republic of Serbia, Project Nos. III45019 and 172007, and the University of Defense, Project No. VA-TT/4-16-18.

The authors have declared no conflict of interest.

References

[1] N. Sahiner, S. Demirci, M. Sahiner, S. Yilmaz, H. Al-Lohedan, The use of superporous *p*-(3-Acrylamidopropyl)trimethyl ammonium chloride cryogels for removal of toxic arsenate anions, *J. Environ. Manage*. 2015, *152*, 66–74.

[2] G. M. P. Morrison, G. E. Bately, T. M. Florence, Metal speciation and toxicity, *Chem. Br*. 1989, *25*, 791–795.

[3] T. S. Y. Choong, T. G. Chuah, Y. Robiah, F. L. G. Koay, I. Azni, Arsenic toxicity, health hazards and removal techniques from water: an overview, *Desalination* 2007, *217*, 139–145.

[4] M. Habuda-Stanić, M. Kuleš, B. Kalajdzić, Z. Romić, Quality of groundwater in eastern Croatia: The problem of arsenic pollution, *Desalination* 2007, *210*, 157–162.

[5] R. Zevenhoven, A. B. Mukherjee, P. Bhattacharya, in *Arsenic in Soil and Groundwater Environment, Biochemical Interactions, Health Effects and Remediation* (Eds.: P. Bhattacharya, A. B. Mukherjee, J. Bundschuh, R. Zevenhoven, R. H. Loeppert), Vol. 9, Elsevier, Amsterdam **2007**, pp. 527–531.

[6] D. Lakshmanan, D. Clifford, G. Samanta, Arsenic removal by coagulation with aluminium, iron, titanium and zirconium, *J. Am. Water Works Assoc*. 2008, *100*, 76–79.

[7] P. Pal, S. Zia, A. Pattanayak, P. Bhattacharya, Removal of arsenic from drinking water by chemical precipitation – a modeling and simulation study of the physical–chemical processes, *Water Environ. Res*. 2007, *79*, 357–366.

[8] E. Mohora, S. Rončević, B. Dalmacija, J. Agbaba, M. Watson, E. Karlović, M. Dalmacija, Removal of natural organic matter and arsenic from water by electrocoagulation/flotation continuous flow reactor, *J. Hazard. Mater*. 2012, *235–236*, 257–264.

[9] S. Bordoloi, S. K. Nath, S. Gogoi, R. K. Dutta, Arsenic and iron removal from groundwater by oxidation–coagulation at optimized pH: Laboratory and field studies, *J. Hazard. Mater*. 2013, *260*, 618–626.

[10] M. Röhricht, J. Krisam, U. Weise, U. R. Kraus, R.-A. Düring, Elimination of Carbamazepine, Diclofenac and Naproxen from Treated Wastewater by Nanofiltration, *Clean - Soil Air Water* 2009, *37*, 638–641.

[11] M. C. Shih, An overview of arsenic removal by pressure-driven membrane processes, *Desalination* 2005, *172*, 85–90.

[12] M. M. Gholami, M. A. Mokhtari, A. Aameri, M. R. A. Fard, Application of reverse osmosis technology for arsenic removal from drinking water, *Desalination* 2006, *200*, 725–727.

[13] P. Xu, M. Capito, T. Y. Cath, Selective removal of arsenic and monovalent ions from brackish water reverse osmosis concentrate, *J. Hazard. Mater*. 2013, *260*, 885–891.

[14] G. P. Miller, D. I. Norman, P. L. Frisch, A comment on arsenic species separation using ion exchange, *Water Res*. 2000, *34*, 1397–1402.

[15] D. Mohan, C. U. Pittman, Arsenic removal from water/wastewater using adsorbents - A critical review, *J. Hazard. Mater*. 2007, *142*, 1–53.

Accepted Article

[16] C. Wang, H. Luo, Z. Zhang, Y. Wu, J. Zhang, S. Chen, Removal of As(III) and As(V) from aqueous solutions using nanoscale zero valent iron-reduced graphite oxide modified composites, *J. Hazard. Mater*. 2014, *268*, 124–131.

[17] F. Fu, D. D. Dionysiou, H. Liu, The use of zero-valent iron for groundwater remediation and wastewater treatment: A review, *J. Hazard. Mater*. 2014, *267*, 194–205.

[18] T. A. Saleh, S. Agrawal, V. K. Gupta, Synthesis of MWCNT/MnO_2 and their application for simultaneous oxidation of arsenite and sorption of arsenate, *Appl. Catal., B* 2011, *106*, 46–53.

[19] V. Vaiano, G. Iervolino, D. Sannino, L. Rizzo, G. Sarno, A. Farina, Enhanced photocatalytic oxidation of arsenite to arsenate in water solutions by a new catalyst based on MoO_x supported on TiO_2, *Appl. Catal., B* 2014, *160–161*, 247–253.

[20] S. A. Baig, T. Sheng, Y. Hu, J. Xu, X. Xu, Arsenic Removal from Natural Water Using Low Cost Granulated Adsorbents: A Review, *Clean – Soil Air Water* 2015, *43 (1)*, 13–26.

[21] Mu. Naushad, Z. A. AL Othman, M. R. Khan, S. M. Wabaidur, Removal of Bromate from Water Using De-Acidite FF-IP Resin and Determination by Ultra-Performance Liquid Chromatography-Tandem Mass Spectrometry, *Clean – Soil Air Water* 2013, *41*, 528–533.

[22] M. Naushad, M. R. Khan, Z. A. AL Othman, I. Al Sohaimi, F. Rodriguez-Reinoso, T. M. Turki, R. Ali, Removal of BrO_3^- from drinking water samples using newly developed agricultural waste-based activated carbon and its determination by ultra-performance liquid chromatography-mass spectrometry, *Environ. Sci. Pollut. Res*. 2015, *22*, 15853–15865.

[23] S. M. Alshehri, M. Naushad, T. Ahamad, Z. A. Al Othman, A. Aldalbahi, Synthesis, characterization of curcumin based ecofriendly antimicrobial bio-adsorbent for the removal of phenol from aqueous medium, *Chem. Eng. J.* 2014, *254*, 181–189.

[24] F. Ciesielczyk, P. Bartczak, T. Jesionowski, A comprehensive study of Cd(II) ions removal utilizing high-surface-area binary Mg-Si hybrid oxide adsorbent, *Int. J. Environ. Sci. Technol.* 2015, *12*, 3613–3626.

[25] F. Ciesielczyk, P. Bartczak, K. Wieszczycka, K. Siwinska-Stefanska, M. Nowacka, T. Jesionowski, Adsorption of Ni(II) from model solutions using co-precipitated inorganic oxides, *Adsorption* 2013, *19*, 423–434.

[26] M. Wysokowski, Ł. Klapiszewski, D. Moszyński, P. Bartczak, T. Szatkowski, I. Majchrzak, K. Siwińska-Stefańska, et al., Modification of Chitin with Kraft Lignin and Development of New Biosorbents for Removal of Cadmium(II) and Nickel(II) Ions, *Mar. Drugs* 2014, *12*, 2245–2268.

[27] Z. A. AL-Othman, R. Ali, M. Naushad, Hexavalent chromium removal from aqueous medium by activated carbon prepared from peanut shell: Adsorption kinetics, equilibrium and thermodynamic studies, *Chem. Eng. J.* 2012, *184*, 238–247.

[28] R. Attinti, D. Sarkar, K. R. Barrett, R. Datta, Adsorption of arsenic(V) from aqueous solutions by goethite/silica nanocomposite, *Int. J. Environ. Sci. Technol.* 2015, *12*, *3905–3914.*

[29] T. R. Roth, K. J. Reddy, in *Natural Arsenic in Groundwaters of Latin America* (Ed.: J. Bundschuh), Taylor & Francis, London **2008**.

[30] C. Colella, in *Natural Zeolites for the Third Millennium*, (Ed.: F. A. Mumpton.), De Frede-Editore, Naples **2000**.

[31] C. A. Martinson, K. J. Reddy, Adsorption of arsenic(III) and arsenic(V) by cupric oxide nanoparticles, *J. Colloid Interface Sci*. 2009, *336*, 406–411.

[32] M. Shahmiri, N. A. Ibrahim, N. Zainuddin, N. Asim, B. Bakhtyar, A. Zaharim, K. Sopian, Effect of pH on

Accepted Article

the synthesis of CuO nanosheets by quick precipitation method, *WSEAS Trans. Environ. Dev.* 2013, *9 (2)*, 137–146.

[33] S. A. Jafari, S. Cheraghi, M. Mirbakhsh, R. Mirza, A. Maryamabadi, Employing Response Surface Methodology for Optimization of Mercury Bioremediation by Vibrio para-haemolyticus PG02 in Coastal Sediments of Bushehr, Iran, *Clean − Soil Air Water* 2015, *43 (1)*, 118–126.

[34] G. Schmid (Ed.), *Nanoparticles: From Theory to Application*, Wiley, Weinheim **2006**.

[35] J. S. Markovski, D. D. Marković, V. R. Đokić, M. Mitrić, M. Đ. Ristić, A. E. Onjia, A. D. Marinković, Arsenate adsorption on waste eggshell modified by goethite, α-MnO_2 and goethite/α-MnO_2, *Chem. Eng. J.* 2014, *237*, 430–442.

[36] P. Scherrer, Bestimmung der Größe und der inneren Struktur von Kolloidteilchen mittels Röntgenstrahlen, *Nachr. Ges. Wiss. Göttingen* 1918, *2*, 98–100.

[37] J. S. Markovski, V. Djokić, M. Milosavljević, M. Mitric, A. A. Perić-Grujić, A. E. Onjia, A. D. Marinković, Ultrasonic assisted arsenate adsorption on solvothermally synthesized calcite modified by goethite, α-MnO_2 and goethite/α-MnO_2, *Ultrason. Sonochem*. 2014, *21*, 790–801.

[38] J. Hong, Z. Zhu, H. Lu, Y. Qiu, Synthesis and arsenic adsorption performances of ferric-based layered double hydroxide with α-alanine intercalation, *Chem. Eng. J*. 2014, *252*, 267–274.

[39] K. Y. Foo, B. H. Hameed, Review: Insights into the modeling of adsorption isotherm systems, *Chem. Eng. J*. 2010, *156*, 2–10.

[40] P. Bartczak, M. Norman, Ł. Klapiszewski, N. Karwańska, M. Kawalec, M. Baczyńska, M. Wysokowski, et al., Removal of nickel(II) and lead(II) ions from aqueous solution using peat as a low-cost adsorbent: A kinetic and equilibrium study, *Arab. J. Chem.* 2015.

[41] Ł. Klapiszewski, P. Bartczak, M. Wysokowski, M. Jankowska, K. Kabat, Silica conjugated with Kraft lignin and its use as a novel 'green'sorbent for hazardous metal ions removal, *Chem. Eng. J.* 2015, 260, 684–693.

[42] A. Goswami, P. K. Raul, M. K. Purkait, Arsenic adsorption using copper(II) oxide nanoparticles. *Chem. Eng. Res. Design*, 2012, *90 (9)*, 1387–1396.

[43] C. A. Martinson, K. J. Reddy, Adsorption of arsenic(III) and arsenic(V) by cupric oxide nanoparticles, *J. Colloid Interface Sci*. 2009, *336*, 406--411.

[44] M. A. Malana, R. B. Qureshi, M. N. Ashiq, Adsorption studies of arsenic on nano aluminium doped manganese copper ferrite polymer (MA, VA, AA) composite: Kinetics and mechanism, *Chem. Eng. J.* 2011, *172 (2–3)*, 721–727.

[45] P. Pillewan, S. Mukherjee, T. Roychowdhury, S. Das, A. Bansiwal, S. Rayalu, Removal of As(III) and As(V) from water by copper oxide incorporated mesoporous alumina, *J. Hazard. Mater.* 2011, *186 (1)*, 367–375.

[46] Z. Veličković, G. D. Vuković, A. D. Marinković, M. S. Moldovan, A. A. Perić-Grujić, P. S. Uskoković, M. Đ. Ristić, Adsorption of arsenate on iron(III) oxide coated ethylenediamine functionalized multiwall carbon nanotubes, *Chem. Eng. J*. 2012, *181–182*, 174–181.

[47] S. Sarkar, L. M. Blaney, A. Gupta, D. Ghosh, A. K. SenGupta, Use of $ArsenX^{np}$, a hybrid anion exchanger, for arsenic removal in remote villages in the Indian subcontinent, *React. Funct. Polym*. 2007, *67*, 1599–1611.

Accepted Article

Figure 1. Contour diagram represent the adsorbent capacity vs. C[$CuCl_2$] and C[$NaBH_4$] (C_i = 0.1 mg L^{-1} As(V), m/V = 100 mg L^{-1}, pH 6, T = 25 °C) a); and capacity of T–Cu(A) sorbent vs. amount of copper loading b) ($C_{[CuCl_2]}$ 0.4–1.2 mol L^{-1} and $C_{[NaBH_4]}$ = 0.14 mol L^{-1}).

Figure 2. XRD patterns of a) T(A) and b) T–Cu(A).

Figure 3. Representative SEM images of T–Cu(A–C) (a–c), and HRTEM images of T–Cu(A) adsorbents (d).

Figure 4. FTIR spectra of tufa (a), T–Cu(A) (b), T–Cu(A)/As(V) (c), and T–Cu(A)/As(III) (d).

Figure 5. Effect of pH on As(V) and As(III) adsorption in the presence of T–Cu(A) under magnetic mixing (m) and ultrasound treatment (u).

Figure 6. Adsorption isotherms of As(V) a) and As(III) b) on T–Cu(A) at 20, 30 and 40 °C (C_i = 0.1, 0.2, 0.3, 0.5, 1.0, 2.0, 3.0, 5.0 and 10.0 mg L^{-1}, m/V = 100 mg L^{-1}, pH 6).

Table 1. Specific surface area (S_p), pore volume (V_p), average pore diameter, pH_{PZC} and zeta potential (ζ) of tufa and T–Cu(A-C)

Sorbent		Surface area (S_p) (m^2 g^{-1})	Pore volume (V_p) (cm^3 g^{-1})	Average pore diameter (nm)	pH_{PZC}[a]	Zeta potential (ζ) (mV)[a, b]
T	A	15.54	0.074	87.47	4.2 ± 0.2	pH 4; 5.6 ± 0.3
	B	12.49	0.073	87.12		pH 6; --2.8 ± 0.1
	C	10.47	0.074	86.22		pH 8; --10.2 ± 0.4
T–Cu	A	65.47	0.336	191.96	8.1 ± 0.3	pH 4; 22.1 ± 0.7
	B	52.12	0.311	190.86		pH 6; 16.5 ± 0.6
	C	46.89	0.285	189.22		pH 8; 4.4 ± 0.5

[a] pH_{PZC} and zeta potential values represents mean values from three determination for T–Cu(A);

[b] similar ζ values were obtained for T–Cu(B) and T–Cu(C)

Accepted Article

Table 2. Adsorption isotherms parameters for As(III) and As(V) removal by T–Cu(A)

Isotherm		Linear method			Non-linear method		
		20 °C	30 °C	40 °C	20 °C	30 °C	40 °C
Langmuir type 1		$\frac{C_e}{q_e}=\frac{C_e}{q_m}+\frac{1}{K_L q_m}$			$q_e = q_m \frac{K_L C_e}{1+K_L C_e}$		
q_m (mg/g)	As(III)	68.65	72.19	71.27	67.83	70.49	69.96
	As(V)	92.92	93.09	93.43	104.62	105.4	106.5
K_L (L/g)	As(III)	1.663	1.727	2.081	2.009	2.178	2.570
	As(V)	4.580	4.988	5.370	2.422	2.524	2.605
R^2	As(III)	0.997	0.997	0.998	0.996	0.995	0.995
	As(V)	0.973	0.972	0.969	0.996	0.995	0.995
Jovanovic-Freundlich		$\ln(-\ln(1-\frac{q_e}{q_m}))=n\ln K_{JF}+n\ln C_e$			$q_e = q_m(1-\exp(-(K_{JF}C_e)^n))$		
q_m (mg/g)	As(III)	60.44	63.36	63.76	60.44	63.36	63.76
	As(V)	96.44	98.82	101.8	96.44	98.82	101.8
K_{JF} (L/g)	As(III)	1.627	0.570	0.503	1.640	1.702	1.919
	As(V)	1.593	0.707	0.735	1.611	1.597	1.554
n	As(III)	0.984	1.003	1.013	0.9390	0.8920	0.8710
	As(V)	0.719	1.400	1.439	0.734	0.716	0.703
R^2	As(III)	0.997	0.994	0.994	0.997	0.993	0.993
	As(V)	0.999	0.998	0.999	0.999	0.998	0.999

Table 3. Calculated Gibbs free energy of adsorption, enthalpy, activation energy and entropy for As(III) and As(V) adsorption on T–Cu(A) at 293, 303 and 313 K

Adsorbate	T-Cu	ΔG^0 (kJ mol^{-1})			ΔH^0	ΔS^0
		293 K	303 K	313 K	(kJ mol^{-1})	(J mol^{-1} K^{-1})
As(III)	A	--38.87 ± 0.98	--41.10 ± 1.24	--42.33 ± 1.45	11.98 ± 0.65	174.0 ± 6.3
	B	--38.38 ± 1.14	--39.79 ± 1.18	--41.59 ± 1.58	8.49 ± 0.21	159.7 ± 5.8
	C	--38.43 ± 1.04	--39.82 ± 1.14	--41.66 ± 1.37	8.76 ± 0.28	160.8 ± 6.1
As(V)	A	--40.18 ± 1.22	--41.87 ± 1.35	--43.33 ± 1.28	5.91 ± 0.15	157.3 ± 6.4
	B	--40.81 ± 1.24	--42.42 ± 1.44	--44.01 ± 1.61	6.15 ± 0.19	160.2 ± 5.3
	C	--40.57 ± 1.31	--42.12 ± 1.34	--43.72 ± 1.47	5.63 ± 0.18	157.6 ± 4.0

Accepted Article

Table 4. Efficiency of iAs removal by T–Cu(A and B) in a presence of interfering anion

Adsorbent	pH	iAs[a] (%)	The content of interfering anions (mg L^{-1})					
			$Cr_2O_7^{2-}$	Cl^-	SO_4^{2-}	F^-	NO_3^-	PO_4^{3-}
Model water[b]	5.4		0.3	5.6	14.7	0.1	3.2	10
T–Cu(A)	6.1	As(V) 93%	0.1	5.4	13.5	0.1	3.1	8.6
		As(III) 84%	BDL	5.5	14.1	0.1	3.2	8.1
T–Cu(B)		As(V) 90%	BDL	5.4	13.6	0.1	3.2	8.7
		As(III) 81%	BDL	5.3	14.0	0.1	3.2	8.3

[a] Percent of iAs removal (mean value from three determination);

[b] Anion content in water spiked with 2.5 mg L^{-1} As(V) and As(III); similar trend was obtained for T–Cu(C);

BDL, below detection limit

Table 5. Desorption study

Desorption agent	$C_{desorption\ agent}$ (mol L^{-1})	Arsenate desorbed (%)	iAs[a] desorbed (%)	Arsenate desorbed (%)	Arsenate desorbed (%)
		T–Cu(A)	T–Cu(A)	T–Cu(B)	T–Cu(C)
NaOH	0.2	65	69	67	71
	0.5	78	83	79	84
NaOH/NaCl	0.2/0.2	76	80	79	81
	0.5/0.2	86	92	90	91
	0.5/0.5	89	93	92	91

[a] 50:50 (1 mg L^{-1}) As(V)/As(III)

Accepted Article

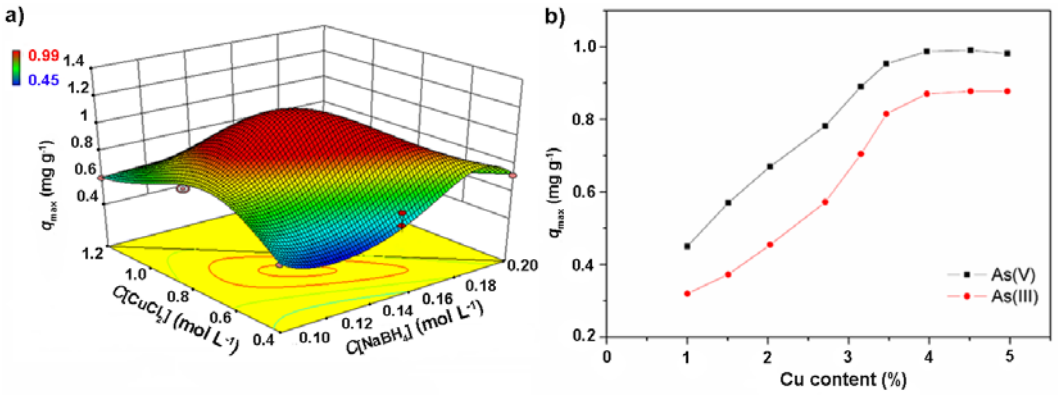

Figure 1

Accepted Article

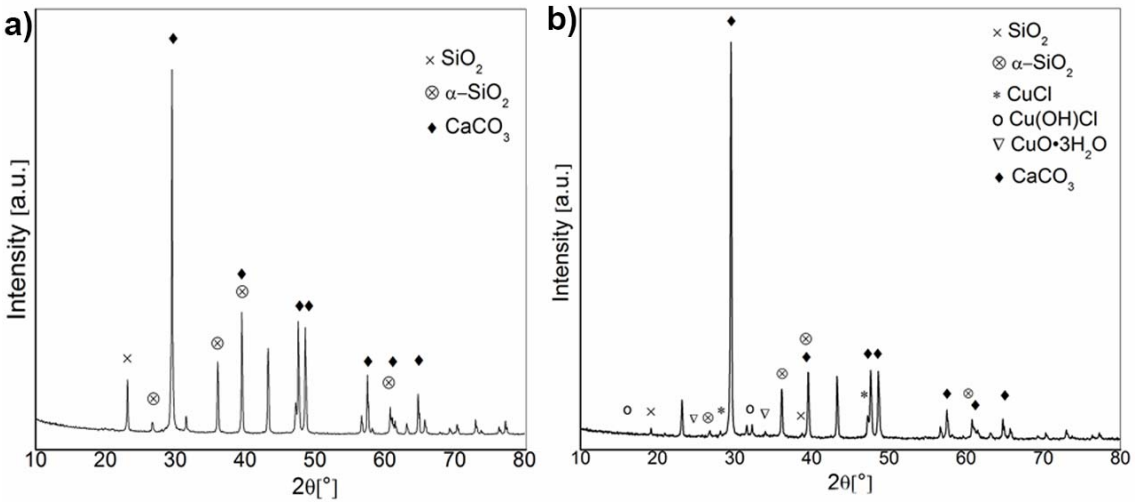

Figure 2

Accepted Article

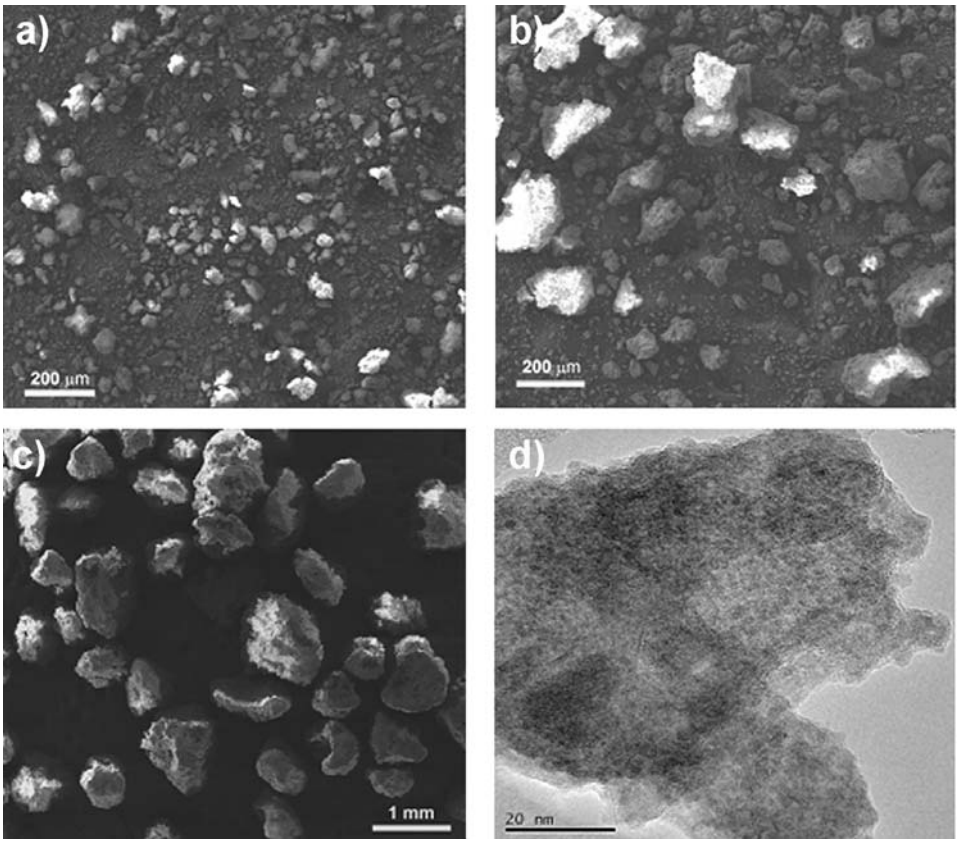

Figure 3

Accepted Article

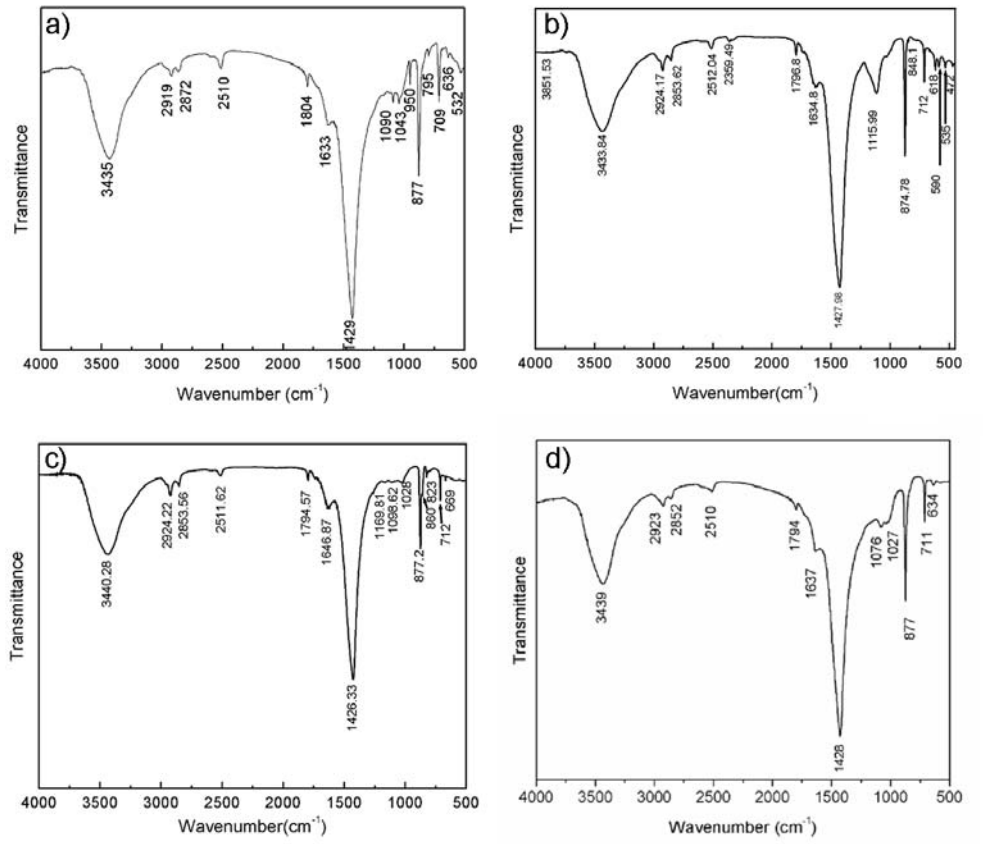

Figure 4

Accepted Article

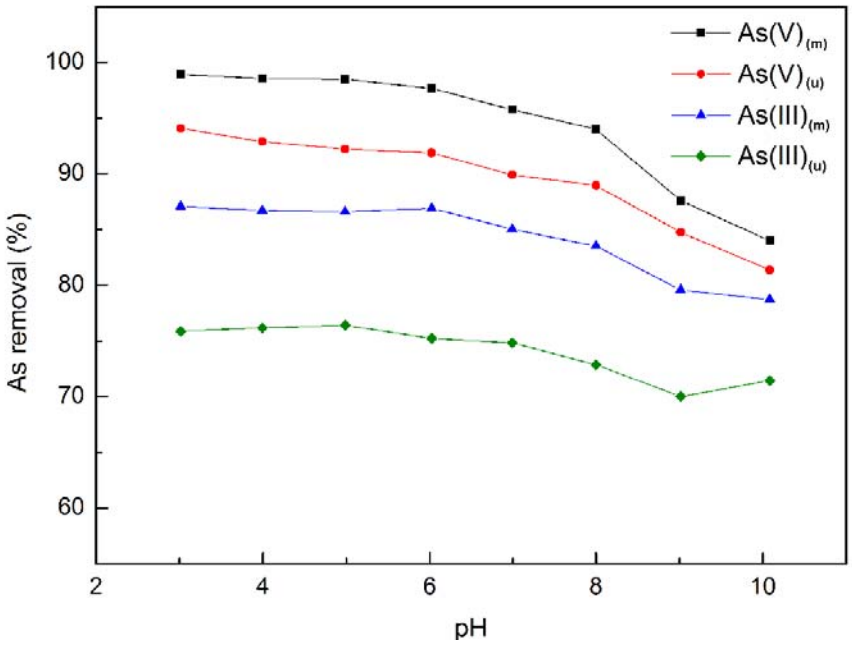

Figure 5

Accepted Article

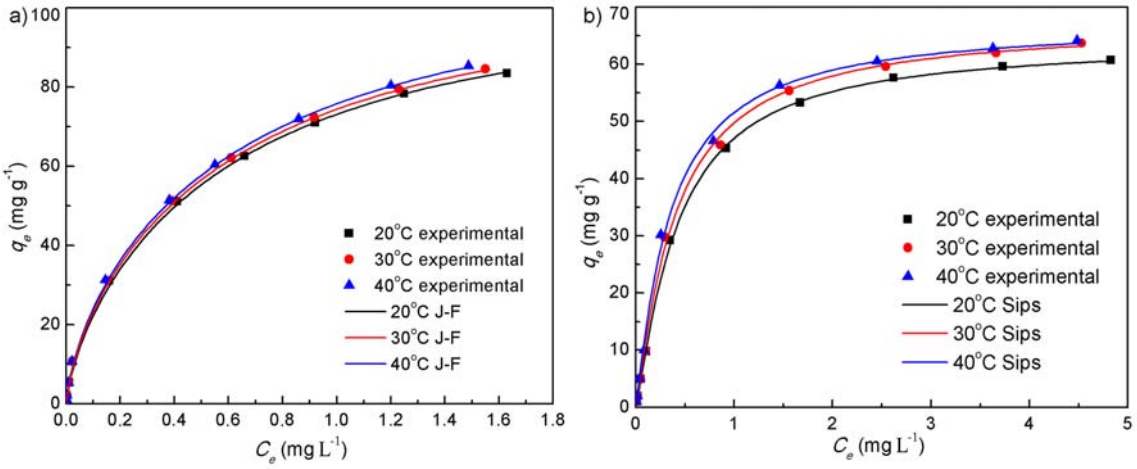

Figure 6